Leveraging Collective Effects for Thermometry in Waveguide Quantum Electrodynamics

Aleksei Sharafiev,[1] Mathieu Juan,[2] Marco Cattaneo,[3] and Gerhard Kirchmair[1,4,*]
[1]Institute for Quantum Optics and Quantum Information, Austrian Academy of Sciences, 6020 Innsbruck, Austria
[2]Institut Quantique and Département de Physique, Université de Sherbrooke, Sherbrooke, Québec, J1K 2R1, Canada
[3]QTF Centre of Excellence, Department of Physics, University of Helsinki, P.O. Box 43, FI-00014 Helsinki, Finland
[4]University of Innsbruck, Institute for Experimental Physics, 6020 Innsbruck, Austria

(Received 15 July 2024; accepted 5 May 2025; published 28 May 2025)

We report a proof-of-principle experiment for a new method of temperature measurements in waveguide quantum electrodynamics experiments, allowing one to measure separately the temperature of global and local baths. The method takes advantage of collective states of two transmons located in the center of a waveguide. The Hilbert space of such a system forms two separate subspaces (bright and dark) that are coupled differently to external noise sources. Measuring transmission through the waveguide allows one to extract separately the temperatures of the baths responsible for global and local excitations in the system. Such a system would allow for building a new type of primary temperature sensor capable of addressing both local and global baths.

DOI: 10.1103/PhysRevLett.134.213602

Characterizing and controlling the coupling between quantum systems and environmental degrees of freedom is one of the central problems in modern quantum systems engineering [1–10]. This coupling might be useful in quantum sensing [11], quantum thermometry [12], or quantum engines [13], while in other applications it is harmful, e.g., for quantum computation protocols, leading to an additional dephasing as well as excess qubit population. The coupling of one quantum system to multiple baths attracted significant attention during the last years on both the theoretical and experimental sides, including the field of superconducting quantum circuits [14–21].

Thermalization of a many body system coupled to various baths is especially relevant in the context of superconducting devices whose effective temperatures are known to plateau at 30–50 mK [22–24]. Various possible reasons for this behavior have been revealed, including poorly thermalized attenuators in the input lines of the cryostat [25,26] as well as nonequilibrium quasiparticles, perhaps produced by stray infrared radiation [27] or cosmic rays [28,29]. Continuing research in this area during the last few years resulted in several proposed and realized protocols for qubit temperature measurements [23,24,30] and techniques for its reduction [31].

To understand the thermal baths that a superconducting circuit is coupled to, one has to perform thermometry on the circuit. Several protocols have been recently proposed [32–35], including realizing a primary thermometer by measuring the scattering parameters of a transmon coupled to a waveguide [36]. The field of thermometry recently expanded to the quantum regime, where entanglement can be used to overcome fundamental limitations of classical thermometry [12]. For instance, exploiting bath-induced correlations may enhance thermometry precision [37].

This Letter introduces a new method for the individual extraction of temperature associated with two noise sources affecting a system of two superconducting transmons, and demonstrates it through a proof-of-principle experiment. Leveraging the inherent symmetry of the system, our approach employs multiprobe spectroscopy to measure separately the temperature of a collective, global bath and of a more localized noise source. In this context, we will employ the term "global" to denote a thermal reservoir symmetrically coupled to both transmons, whereas "local" refers to a noise source that is more strongly coupled to one transmon, thereby inducing an asymmetry in the dissipation channels. The latter scenario encompasses purely localized baths extensively examined in theoretical studies [16,17,38–40], wherein noise sources exclusively affect a single transmon.

Our method introduces a contribution to the toolbox of existing cryogenic thermometry protocols, offering a novel capability of dealing with both local and global noise sources. Our approach holds the potential to emerge as an indispensable tool for detecting different noise sources influencing superconducting qubits. Such a tool allows the design of countermeasures and leads to a better

*Contact author: gerhard.kirchmair@uibk.ac.at

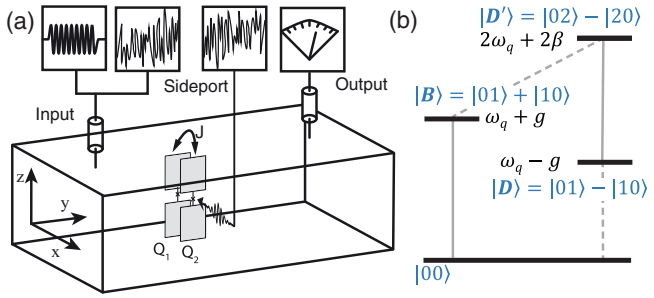

FIG. 1. (a) Experimental setup: a rectangular waveguide (global bath) with two transmons. (b) Simplified level scheme of the two transmons with the corresponding states (normalization omitted). Solid lines correspond to allowed transitions in the global regime, while dashed lines correspond to prohibited ones. Only one level with two excitations $|D'\rangle$ is shown. Levels $|D'\rangle$ and $|D\rangle$ belong to the dark subspace, while $|00\rangle$ and $|B\rangle$ belong to the bright subspace. Notations: $2\beta < 0$, anharmonicity of the transmons with frequencies ω_q; $g > 0$, capacitive coupling between the transmons.

understanding of the complex thermalization of extended circuits.

Our experimental setup is shown in Fig. 1(a), where two capacitively coupled flux tunable transmons (Q_1 and Q_2) are located in the center of a rectangular waveguide (see [41,42]). The waveguide cutoff frequency was close to 6.5 GHz for the fundamental mode and 13 GHz for the second mode. For the experiment, the system was equipped with two electromagnets thermally anchored to a base plate of a dilution refrigerator (not shown), allowing for an independent control of the transmons frequencies from around 4 to 8 GHz. The transmons were fabricated with a standard $Al/AlO_x/Al$ bridge-free technique [43] on 330 μm-thick sapphire substrate.

Owing to the symmetry of the system, we separate the two-transmon Hilbert space into a *dark* or *subradiant* subspace, which is effectively decoupled from the noise coming through the waveguide, and a *bright* or *superradiant* subspace [9,14,44] [see Fig. 1(b)]. In addition, a pin mounted on the side of the waveguide weakly couples to both transmons. This line is used to engineer a controlled thermal bath acting on the transmons, whose effective temperature can be varied in a broad range (roughly from 100 mK to 60 K with the noise source we used). Crucially, owing to the asymmetry of the evanescent field of the pin, this bath couples to both dark and bright subspaces.

In the following, the bath associated with the pin line will be referred to as "local" in contrast to the bath associated with the fundamental mode of the waveguide, which we will call "global." A 3D waveguide QED setup was chosen to have an alternative way to engineer the local bath with a heater affecting only one qubit [see details in Supplemental Material (SM) [45]]. The system was designed in a way to have unequal couplings to different baths: $\gamma_{\mathrm{loc1}} < \gamma_{\mathrm{loc2}} \ll \gamma_{\mathrm{glob}}$. A more strongly coupled global bath corresponds to a typical experimental situation in waveguide QED, while local baths can be associated with internal losses. Having the transmon pair coupled strongly to the global bath of a continuous mode environment makes the system more sensitive to its temperature, in turn leading to a higher residual temperature for the transmons. For this proof-of-principle experiment this situation is acceptable as this residual temperature, associated with the microwave photons in the input line, can be easily included in the model. Even more so it is close to a relevant measurement scenario where one wants to determine the mode temperature of a transmission line connecting to an experiment to ensure proper filtering and attenuation. A waveguide setup allows a directly measurable coupling to an incoming thermal radiation field and an absolute temperature measurement [36] of this mode. Here, the local bath (e.g., a residual bulk temperature) would be a detrimental influence, limiting the measurement if one uses a single transmon, which is eliminated in our setup.

The system illustrated in Fig. 1(a) has three ports: input and output of the waveguide, connected correspondingly to standard 50 Ω input and output lines, and the side pin line, connected to a second standard 50 Ω input line. A detailed microwave wiring can be found in SM [45]. To couple our system to a bath (local or global) we apply controlled white noise to the corresponding port, produced by amplifying the Johnson noise of a 50 Ω load with a room temperature amplifier chain combined with a digital attenuator. By changing the settings of the attenuator we effectively regulate the noise temperature.

As we can send noise separately to the different input ports, we are able to independently study the global and local baths. The effect of each bath is obtained by measuring the transmission through the waveguide, which depends on the steady state of the transmons [56], and thus their temperatures. Because of the presence of a dark subspace with respect to the global case, the transmission coefficient in this scenario will be crucially different from the local bath case where the dark state is broken. Through a suitable fit of these coefficients we can then extract the temperatures of the baths independently.

For a theoretical description of our model (see details in SM [45]), we will model the effect of the baths on the two-transmon system through a Bloch-Redfield master equation in a partial secular approximation [17,57], whose Markovianity is justified by the approximately flat spectral density of the baths (see SM [45] for some related considerations) and by the weak coupling between transmons and reservoirs, combined with input-output formalism [56]. We can understand the behavior of the transmission coefficients in the global and local scenarios by looking at the simplified level scheme in Fig. 1(b) (a more detailed scheme can be found in SM [45]): under the action of a perfectly symmetric global bath, the levels $|D\rangle$ and $|D'\rangle$ are decoupled from the other levels as the

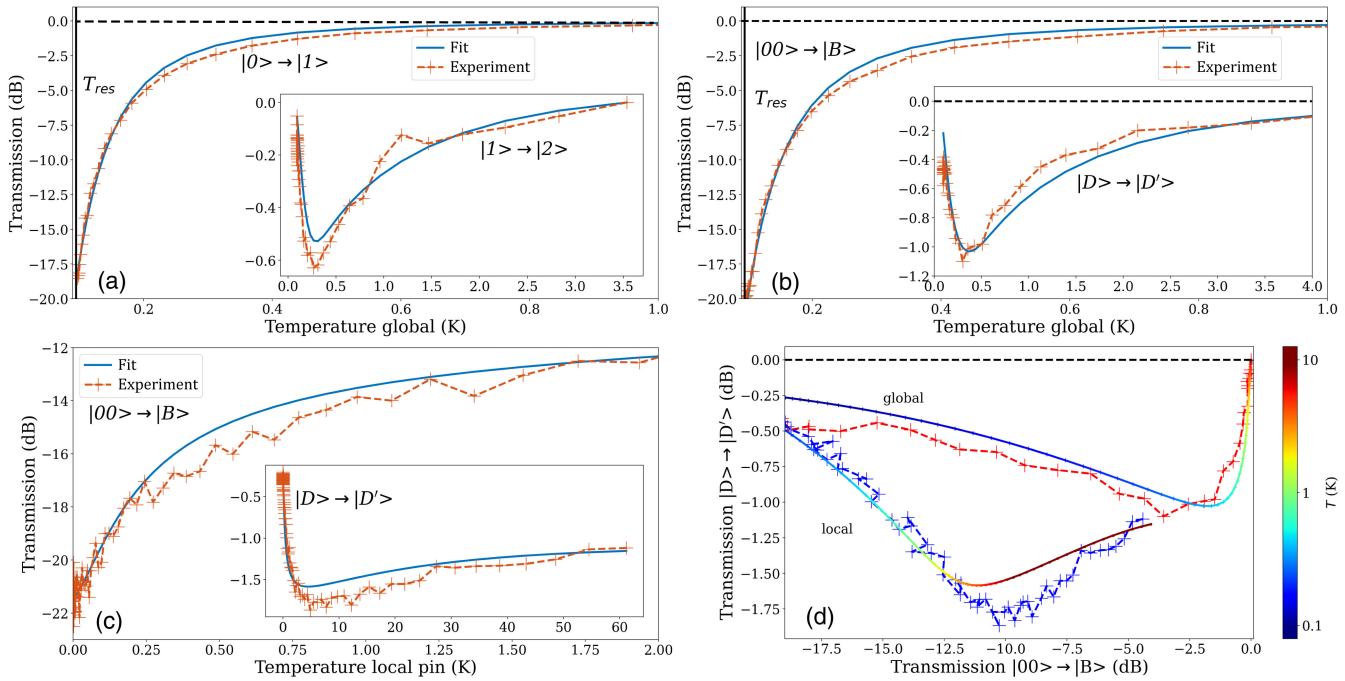

FIG. 2. Transmission measurements (dashed red) and corresponding fitting curves (solid blue) for (a) single transmon, only global bath applied; (b) two transmons in resonance, only global bath applied; and (c) two transmons in resonance, only local bath applied. (d) Bright-dark diagram obtained from (b) and (c). Dashed red (blue): transmission measurements with a global (local) bath. The color of the solid lines (theoretical predictions) reflects the temperature of the corresponding bath.

transitions are prohibited by symmetry. These levels therefore will not be populated by a global bath, regardless of the temperature of the bath. On the other hand, a bath that is coupled only to one transmon (or asymmetrically to both transmons) breaks the symmetry and therefore can populate the $|D\rangle$ state.

Note that the $|D\rangle \rightarrow |D'\rangle$ transition is allowed even under the action of a symmetric global bath, and therefore can be probed through transmission measurements. The visibility of this transition depends directly on the steady state coherences induced by the drive field between $|D\rangle$ and $|D'\rangle$ (see more details in SM [45]), which are zero if the state $|D\rangle$ is not populated. These coherences effectively result in a coherent scattering of the weak incoming field such that one has destructive interference between the scattered and incoming field in forward direction, effectively resulting in low (negative dB value) transmission. As a result, the transmission through the waveguide for frequencies corresponding to the $|00\rangle \rightarrow |B\rangle$ and $|D\rangle \rightarrow |D'\rangle$ transitions can be used to extract the temperatures of both global and local baths independently. In our experiment, the anharmonicities of the transmons are nonidentical [58], therefore the coupling to the global bath is not perfectly symmetric. Measuring the transition rates and fitting them with an adequate model, allows an independent temperature estimation also in such a nonideal real-life setup.

First, we calibrate the power reaching the transmons from the two input ports, using a simple Autler-Towns experiment (see SM [45]). For this, we apply a coherent tone to the corresponding input in resonance with one of the transmons while the other transmon is detuned below the cutoff of the waveguide. As a result, the transmon frequency splits and the width of the splitting is proportional to the Rabi frequency. Then, we fit the effects of the noise source power on one of the transmons (Q_2) to calibrate the effective temperature of the bath. The model has two fitting parameters: residual temperature T_{res} and conversion coefficient α between the power of the source and added noise temperature, i.e., $T = T_{\mathrm{res}} + \alpha P$, where P is the power we send into the fridge. We estimate these values by getting the best possible fit of our theoretical model to the experimental transmission coefficients as a function of temperature of the global bath for the main transition $|0\rangle \rightarrow |1\rangle$ (see SM [45]) for a bath with temperature T. The results of the experiment and their best theoretical fit are shown in Fig. 2(a). The extracted value of T_{res} is 95 mK with a base temperature of the fridge of 14 mK. We associate this relatively high value with the influence of a residual global bath, i.e., photons coming from the input port of the waveguide. This result is expected in waveguide QED experiments, where the transmons are placed in a continuous 50 Ω environment.

Then, we compute the transmission coefficients of different transitions for the single- and two-transmon systems as a function of temperature using our theoretical model with the fit values for T_{res} and α, and compare them with the experimental results. The good agreement between

the experimental and theoretical lines shows that our theoretical model is a good description of the experiment, as can be seen for instance in the inset in Fig. 2(a) for the transmission coefficients of the $|1\rangle \rightarrow |2\rangle$ transition or Fig. 2(b) for the $|00\rangle \rightarrow |B\rangle$ transition. The behavior of the transmission coefficients as a function of temperature is discussed in more detail in the End Matter.

Next, we set both transmons in resonance at 7.8 GHz and vary the noise temperature of both global and local baths. In this case we are interested in two transitions: $|00\rangle \rightarrow |B\rangle$ and $|D\rangle \rightarrow |D'\rangle$; see Fig. 1(a). We start by varying the temperature of the global bath and monitoring the transmission at the f_{00B} and $f_{DD'}$ frequencies with a weak probe. The result of the experiment and the corresponding theoretical lines are shown in Fig. 2(b). We refer to the End Matter for a discussion on the temperature dependence of these transmission coefficients.

In a device with a perfect symmetry, the global bath temperature would not affect the transmission through the waveguide at the $|D\rangle \rightarrow |D'\rangle$ frequency $f_{DD'}$. In our setup a dependence on temperature appears both in the experiment and the theoretical fit (the transmission coefficients are lower than 1), as demonstrated in the inset of Fig. 2(b). This is due to experimental imperfections and additional levels and is discussed further in the End Matter.

Finally we use the side pin to apply a local bath, affecting the transmons asymmetrically. Performing an Autler-Towns experiment, but applying the pump tone from the side pin, we were able to extract the ratio of the couplings between the transmons and the side pin, obtaining $\gamma_{\mathrm{loc2}}/\gamma_{\mathrm{loc1}} = 1.78$. This ratio was used in the model, while the coupling itself was kept as a fitting parameter. To extract the coupling we again fit only single-transmon data, which in this case is fitted simultaneously for both transmons. For the details on this procedure see SM [45]. After extracting the coupling, we plot the experimental and theoretical results for the two transmons and local bath experiment in Fig. 2(c). As before, the theoretical lines are obtained with the values of T_{res} and α fitted in single-transmon experiments.

We observe that for the local bath the transmission drop is deeper and occurs when the $|00\rangle \rightarrow |B\rangle$ transmission is far from reaching saturation (more discussions about this in the End Matter). This can be better illustrated with what we call "bright-dark diagram"; see Fig. 2(d), where the axes correspond to the transmission values at the frequencies f_{00B} and $f_{DD'}$. Experimental frequency sweeps in SM [45] further illustrate the difference between the effects of global and local baths on the transmission.

From this diagram one can see that local and global bath saturate the transitions $|D\rangle \rightarrow |D'\rangle$ and $|00\rangle \rightarrow |B\rangle$ very differently. Thus, a combined measurement allows us to assess the influence of a local bath on a temperature measurement using the $|00\rangle \rightarrow |B\rangle$ as a calibrated sensor. In our proof-of-principle experiment, where both baths have been calibrated, we can actually determine the temperature of both uniquely by measuring the depth of both spectroscopy peaks. This works for a temperature range of 50 mK to about 500 mK for the global and 100 mK to about 2 K for the local baths. Using the qubit pair as a sensor to determine the effective mode temperature of an incoming coaxial line (a global bath) one would not be able to determine the temperature of the local bath as the coupling would not be known. Still our method would allow one to extract its influence on the measurement signal, correct for it, and determine the actual mode temperature.

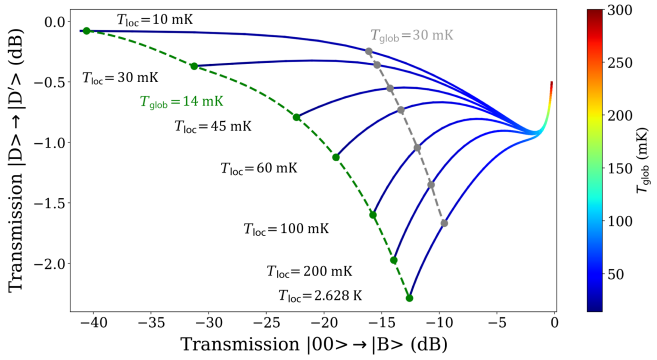

FIG. 3. Theoretical bright-dark diagrams for an experiment with low frequency (2 GHz) transmons. All lines correspond to T_{glob} change from 10 to 300 mK.

To illustrate the measurement process further we have run simulations of a system based on our experiment that is suitable to detect the desired low input mode temperatures (≈20 mK) of a circuit quantum electrodynamics system. The results of this simulation can be seen in Fig. 3. Here, we change the global bath temperature from 10 to 300 mK for a pair of 2 GHz transmons inside a waveguide. We assume a local bath coupling of 1 kHz with other parameters corresponding to our current experiment. Again, a combined measurement of both transitions allows one to determine the temperature of the global bath and extract the influence of the local bath.

From the level diagram [see Fig. 1(b)], one can see that the local bath has a very strong influence on the temperature measurement using the transmission on the $|00\rangle \rightarrow |B\rangle$, leading to a wrong inference of the global bath temperature when only this transition is used. This is the same situation for thermometry methods based on a single transmon: local and global baths cannot be differentiated, making it impossible to definitively identify the origin of excess temperature in the system. From the measurement of the $|D\rangle \rightarrow |D'\rangle$ one can determine the residual excitation of the transmons due to a local bath and correct for it in the global bath measurement. In other words for a well calibrated two-transmon sensor with a verified model, each "line" in the bright-dark diagram can be uniquely associated with a combined measurement of the $|D\rangle \rightarrow |D'\rangle$ and

$|00\rangle \rightarrow |B\rangle$ lines. Two dashed lines in Fig. 3 corresponding to global bath temperature 14 and 30 mK serve as guide to the eye and correspond to typical base plate temperature of a dilution refrigerator and a lowest residual transmon frequency typically observed experimentally. Some more details are provided in SM [45].

In conclusion, we have demonstrated a proof-of-principle setup that allows for the separate temperature estimation of either a local or global bath coupled to a quantum sensor by measuring two transitions of the coupled system. We achieve this by exploiting system symmetries combined with a good calibration of the system and a fit to a theory model. Developing this proof-of-principle experiment into a useful thermometer that would accurately measure the input mode temperature of a system and be able to correct for undesired local bath couplings would require switching to a coplanar waveguide architecture as manufacturing tolerances leading to asymmetries and impedance matching could be improved. We believe the approach presented in this Letter opens a promising avenue for a new type of primary temperature sensor capable of separately deal with local and global baths for temperatures as low as ~20–30 mK, enabling more accurate temperature measurements.

Acknowledgments—The authors would like to thank Roberta Zambrini for useful comments on the theoretical model employed in this work. M. C. would like to thank the members of the PICO group at Aalto University for interesting discussions and suggestions. A. S. and G. K. acknowledge funding by the European Research Council (ERC) under the European Union Horizon 2020 research and innovation program (714235). This research was funded in part by the Austrian Science Fund (FWF) [grant DOI: 10.55776/F71]. M. C. acknowledges funding from the Research Council of Finland Centre of Excellence program grant 336810 and from COQUSY project PID2022-140506NB-C21 funded by MCIN/AEI/10.13039/501100011033. M. L. J. acknowledges funding by the Canada First Research Excellence Fund.

Data availability—The data that support the findings of this study are available on Zenodo [59].

[1] K. W. Murch, U. Vool, D. Zhou, S. J. Weber, S. M. Girvin, and I. Siddiqi, Cavity-assisted quantum bath engineering, Phys. Rev. Lett. **109**, 183602 (2012).

[2] A. Soare, H. Ball, D. Hayes, X. Zhen, M. C. Jarratt, J. Sastrawan, H. Uys, and M. J. Biercuk, Experimental bath engineering for quantitative studies of quantum control, Phys. Rev. A **89**, 042329 (2014).

[3] C. Aron, M. Kulkarni, and H. E. Türeci, Steady-state entanglement of spatially separated qubits via quantum bath engineering, Phys. Rev. A **90**, 062305 (2014).

[4] M. E. Kimchi-Schwartz, L. Martin, E. Flurin, C. Aron, M. Kulkarni, H. E. Tureci, and I. Siddiqi, Stabilizing entanglement via symmetry-selective bath engineering in superconducting qubits, Phys. Rev. Lett. **116**, 240503 (2016).

[5] A. Shabani and H. Neven, Artificial quantum thermal bath: Engineering temperature for a many-body quantum system, Phys. Rev. A **94**, 052301 (2016).

[6] S. Campbell, M. Mehboudi, G. D. Chiara, and M. Paternostro, Global and local thermometry schemes in coupled quantum systems, New J. Phys. **19**, 103003 (2017).

[7] P. M. Harrington, M. Naghiloo, D. Tan, and K. W. Murch, Bath engineering of a fluorescing artificial atom with a photonic crystal, Phys. Rev. A **99**, 052126 (2019).

[8] C. L. Latune, I. Sinayskiy, and F. Petruccione, Collective heat capacity for quantum thermometry and quantum engine enhancements, New J. Phys. **22**, 083049 (2020).

[9] M. Cattaneo, G. L. Giorgi, S. Maniscalco, G. S. Paraoanu, and R. Zambrini, Bath-induced collective phenomena on superconducting qubits: Synchronization, subradiance, and entanglement generation, Ann. Phys. (Berlin) **533**, 2100038 (2021).

[10] J. M. Kitzman, J. R. Lane, C. Undershute, P. M. Harrington, N. R. Beysengulov, C. A. Mikolas, K. W. Murch, and J. Pollanen, Phononic bath engineering of a superconducting qubit, Nat. Commun. **14**, 1 (2023).

[11] C. L. Degen, F. Reinhard, and P. Cappellaro, Quantum sensing, Rev. Mod. Phys. **89**, 035002 (2017).

[12] A. De Pasquale and T. M. Stace, Quantum thermometry, in *Thermodynamics in the Quantum Regime: Fundamental Aspects and New Directions*, edited by F. Binder, L. A. Correa, C. Gogolin, J. Anders, and G. Adesso (Springer International Publishing, Cham, 2018), pp. 503–527.

[13] L. M. Cangemi, C. Bhadra, and A. Levy, Quantum engines and refrigerators, Phys. Rep. **1087**, 1 (2024).

[14] B. Karimi and J. P. Pekola, Correlated versus uncorrelated noise acting on a quantum refrigerator, Phys. Rev. B **96**, 115408 (2017).

[15] L.-Z. Hu, Z.-X. Man, and Y.-J. Xia, Steady-state entanglement and thermalization of coupled qubits in two common heat baths, Quantum Inf. Process. **17**, 45 (2018).

[16] P. P. Hofer, M. Perarnau-Llobet, L. D. M. Miranda, G. Haack, R. Silva, J. B. Brask, and N. Brunner, Markovian master equations for quantum thermal machines: Local versus global approach, New J. Phys. **19**, 123037 (2017).

[17] M. Cattaneo, G. L. Giorgi, S. Maniscalco, and R. Zambrini, Local versus global master equation with common and separate baths: Superiority of the global approach in partial secular approximation, New J. Phys. **21**, 113045 (2019).

[18] M. Cattaneo and G. S. Paraoanu, Engineering dissipation with resistive elements in circuit quantum electrodynamics, Adv. Quantum Technol. **4**, 2100054 (2021).

[19] A. Ronzani, B. Karimi, J. Senior, Y.-C. Chang, J. T. Peltonen, C. Chen, and J. P. Pekola, Tunable photonic heat transport in a quantum heat valve, Nat. Phys. **14**, 991 (2018).

[20] U. von Lüpke, F. Beaudoin, L. M. Norris, Y. Sung, R. Winik, J. Y. Qiu, M. Kjaergaard, D. Kim, J. Yoder, S. Gustavsson, L. Viola, and W. D. Oliver, Two-qubit spectroscopy of spatiotemporally correlated quantum noise in superconducting qubits, PRX Quantum **1**, 010305 (2020).

[21] J. Senior, A. Gubaydullin, B. Karimi, J. T. Peltonen, J. Ankerhold, and J. P. Pekola, Heat rectification via a superconducting artificial atom, Commun. Phys. **3**, 1 (2020).
[22] A. D. Córcoles, J. M. Chow, J. M. Gambetta, C. Rigetti, J. R. Rozen, G. A. Keefe, M. Beth Rothwell, M. B. Ketchen, and M. Steffen, Protecting superconducting qubits from radiation, Appl. Phys. Lett. **99**, 181906 (2011).
[23] X. Y. Jin, A. Kamal, A. P. Sears, T. Gudmundsen, D. Hover, J. Miloshi, R. Slattery, F. Yan, J. Yoder, T. P. Orlando, S. Gustavsson, and W. D. Oliver, Thermal and residual excited-state population in a 3D transmon qubit, Phys. Rev. Lett. **114**, 240501 (2015).
[24] A. Kulikov, R. Navarathna, and A. Fedorov, Measuring effective temperatures of qubits using correlations, Phys. Rev. Lett. **124**, 240501 (2020).
[25] J.-H. Yeh, J. LeFebvre, S. Premaratne, F. C. Wellstood, and B. S. Palmer, Microwave attenuators for use with quantum devices below 100 mK, J. Appl. Phys. **121**, 224501 (2017).
[26] S. Krinner, S. Storz, P. Kurpiers, P. Magnard, J. Heinsoo, R. Keller, J. Lütolf, C. Eichler, and A. Wallraff, Engineering cryogenic setups for 100-qubit scale superconducting circuit systems, Eur. Phys. J. Quantum Technol. **6**, 1 (2019).
[27] R. Barends, J. Wenner, M. Lenander, Y. Chen, R. C. Bialczak, J. Kelly, E. Lucero, P. O'Malley, M. Mariantoni, D. Sank, H. Wang, T. C. White, Y. Yin, J. Zhao, A. N. Cleland, J. M. Martinis, and J. J. A. Baselmans, Minimizing quasiparticle generation from stray infrared light in superconducting quantum circuits, Appl. Phys. Lett. **99**, 113507 (2011).
[28] F. Henriques, F. Valenti, T. Charpentier, M. Lagoin, C. Gouriou, M. Martínez, L. Cardani, M. Vignati, L. Grünhaupt, D. Gusenkova, J. Ferrero, S. T. Skacel, W. Wernsdorfer, A. V. Ustinov, G. Catelani, O. Sander, and I. M. Pop, Phonon traps reduce the quasiparticle density in superconducting circuits, Appl. Phys. Lett. **115**, 212601 (2019).
[29] M. McEwen *et al.*, Resolving catastrophic error bursts from cosmic rays in large arrays of superconducting qubits, Nat. Phys. **18**, 107 (2022).
[30] P. Krantz, A. Bengtsson, M. Simoen, S. Gustavsson, V. Shumeiko, W. D. Oliver, C. M. Wilson, P. Delsing, and J. Bylander, Single-shot read-out of a superconducting qubit using a Josephson parametric oscillator, Nat. Commun. **7**, 1 (2016).
[31] M. Lucas, A. V. Danilov, L. V. Levitin, A. Jayaraman, A. J. Casey, L. Faoro, A. Y. Tzalenchuk, S. E. Kubatkin, J. Saunders, and S. E. de Graaf, Quantum bath suppression in a superconducting circuit by immersion cooling, Nat. Commun. **14**, 3522 (2023).
[32] B. Karimi and J. P. Pekola, Noninvasive thermometer based on the zero-bias anomaly of a superconducting junction for ultrasensitive calorimetry, Phys. Rev. Appl. **10**, 054048 (2018).
[33] L. B. Wang, O.-P. Saira, and J. P. Pekola, Fast thermometry with a proximity Josephson junction, Appl. Phys. Lett. **112**, 013105 (2018).
[34] J. Wheeler, M. R. Vissers, M. Malnou, J. Hubmayr, J. N. Ullom, and J. Gao, Sub-Kelvin thermometer for on-chip measurements of microwave devices utilizing two-level systems in superconducting microresonators, Appl. Phys. Lett. **117**, 192601 (2020).
[35] F. Blanchet, Y.-C. Chang, B. Karimi, J. T. Peltonen, and J. P. Pekola, Radio-frequency Coulomb-blockade thermometry, Phys. Rev. Appl. **17**, L011003 (2022).
[36] M. Scigliuzzo, A. Bengtsson, J.-C. Besse, A. Wallraff, P. Delsing, and S. Gasparinetti, Primary thermometry of propagating microwaves in the quantum regime, Phys. Rev. X **10**, 041054 (2020).
[37] G. Planella, M. F. B. Cenni, A. Acín, and M. Mehboudi, Bath-induced correlations enhance thermometry precision at low temperatures, Phys. Rev. Lett. **128**, 040502 (2022).
[38] A. Levy and R. Kosloff, The local approach to quantum transport may violate the second law of thermodynamics, Europhys. Lett. **107**, 20004 (2014).
[39] A. S. Trushechkin and I. V. Volovich, Perturbative treatment of inter-site couplings in the local description of open quantum networks, Europhys. Lett. **113**, 30005 (2016).
[40] J. O. González, L. A. Correa, G. Nocerino, J. P. Palao, D. Alonso, and G. Adesso, Testing the validity of the "local" and "global" GKLS master equations on an exactly solvable model, Open Syst. Inf. Dyn. **24**, 1740010 (2017).
[41] A. Sharafiev, M. L. Juan, O. Gargiulo, M. Zanner, S. Wögerer, J. J. García-Ripoll, and G. Kirchmair, Visualizing the emission of a single photon with frequency and time resolved spectroscopy, Quantum **5**, 474 (2021).
[42] M. Zanner, T. Orell, C. M. F. Schneider, R. Albert, S. Oleschko, M. L. Juan, M. Silveri, and G. Kirchmair, Coherent control of a multi-qubit dark state in waveguide quantum electrodynamics, Nat. Phys. **18**, 538 (2022).
[43] F. Lecocq, I. M. Pop, Z. Peng, I. Matei, T. Crozes, T. Fournier, C. Naud, W. Guichard, and O. Buisson, Junction fabrication by shadow evaporation without a suspended bridge, Nanotechnology **22**, 315302 (2011).
[44] J.-Q. Liao, J.-F. Huang, and L.-M. Kuang, Quantum thermalization of two coupled two-level systems in eigenstate and bare-state representations, Phys. Rev. A **83**, 052110 (2011).
[45] See Supplemental Material at http://link.aps.org/supplemental/10.1103/PhysRevLett.134.213602, which includes Refs. [46–55], for experimental data obtained with a local heater, more details of the experimental setup, the theoretical model, a detailed spectrum of the system, the parameter extraction for single qubits, and theoretical prediction for different configurations.
[46] A. Blais, A. L. Grimsmo, S. M. Girvin, and A. Wallraff, Circuit quantum electrodynamics, Rev. Mod. Phys. **93**, 025005 (2021).
[47] M. Cattaneo, G. L. Giorgi, S. Maniscalco, and R. Zambrini, Symmetry and block structure of the Liouvillian superoperator in partial secular approximation, Phys. Rev. A **101**, 042108 (2020).
[48] J. Jeske, D. J. Ing, M. B. Plenio, S. F. Huelga, and J. H. Cole, Bloch-Redfield equations for modeling light-harvesting complexes, J. Chem. Phys. **142**, 064104 (2015).
[49] J. Cresser and C. Facer, Coarse-graining in the derivation of Markovian master equations and its significance in quantum thermodynamics, arXiv:1710.09939.
[50] D. Farina and V. Giovannetti, Open-quantum-system dynamics: Recovering positivity of the Redfield equation via

the partial secular approximation, Phys. Rev. A **100**, 012107 (2019).
[51] R. Hartmann and W. T. Strunz, Accuracy assessment of perturbative master equations: Embracing nonpositivity, Phys. Rev. A **101**, 012103 (2020).
[52] C. W. Gardiner and P. Zoller, *Quantum Noise* (Springer, New York, 2000).
[53] A. Sharafiev and M. Cattaneo, `Twotransmons_lvsg`: Code for finding the steady state and transmission coefficients of two transmons in a waveguide interacting with both local and global thermal baths (2024), https://github.com/MarcoCattaneo/TwoTransmons_LvsG.
[54] J. R. Johansson, P. D. Nation, and F. Nori, QuTiP 2: A Python framework for the dynamics of open quantum systems, Comput. Phys. Commun. **184**, 1234 (2013).
[55] D. A. Lidar and K. Birgitta Whaley, Decoherence-free subspaces and subsystems, in *Irreversible Quantum Dynamics*, edited by F. Benatti and R. Floreanini (Springer, Berlin, Heidelberg, 2003), pp. 83–120.
[56] K. Lalumière, B. C. Sanders, A. F. van Loo, A. Fedorov, A. Wallraff, and A. Blais, Input-output theory for waveguide QED with an ensemble of inhomogeneous atoms, Phys. Rev. A **88**, 043806 (2013).
[57] H.-P. Breuer and F. Petruccione, *The Theory of Open Quantum Systems* (Oxford University Press, New York, 2002).
[58] J. Koch, T. M. Yu, J. Gambetta, A. A. Houck, D. I. Schuster, J. Majer, A. Blais, M. H. Devoret, S. M. Girvin, and R. J. Schoelkopf, Charge-insensitive qubit design derived from the Cooper pair box, Phys. Rev. A **76**, 042319 (2007).
[59] A.Sharafiev, M. Juan, M. Cattaneo, and G. Kirchmair, Data that support the finding for this article are available under Zenodo, 10.5281/zenodo.14051836 (2025).

End Matter

Behavior of the transmission coefficients vs T—The behavior of the transmission coefficients as a function of temperature can be understood as follows (for a detailed theoretical description, see SM [45]). These coefficients reflect the presence of coherences between transition levels in the steady state of the two-transmon system, induced by a drive field near the transition frequency. At high temperatures, all transmission coefficients saturate at unity transmission (0 dB) as the system reaches a maximally mixed state, making the output field equal to the input field. For the $|0\rangle \to |1\rangle$ transition, the transmission coefficient is much lower than that at low temperatures. Essentially the qubit can coherently scatter a weak incoming field such that one has destructive interference between the scattered and incoming field in forward direction. For higher temperature the incoherent mixture of $|0\rangle$ and $|1\rangle$ results in a smaller amplitude of coherently scattered light such that this destructive interference does not happen and the transmission increases smoothly toward 1 (0 dB) at infinite temperature, as shown in Fig. 2(a). In contrast, since the $|1\rangle$ level is unpopulated at zero temperature, the transmission coefficient for the $|1\rangle \to |2\rangle$ transition is unity at both zero and infinite temperatures, varying only in the intermediate range, as depicted in the inset of Fig. 2(a).

The same temperature dependence of the transmission coefficients for the transitions $|0\rangle \to |1\rangle$ and $|1\rangle \to |2\rangle$ applies to the transitions $|00\rangle \to |B\rangle$ and $|D\rangle \to |D'\rangle$ in the two-transmon system. Their behavior at $T = 0$ and $T = \infty$ is the same, regardless of the bath type. This explains the transmission coefficient limits in both Figs. 2(b) (global bath) and 2(c) (local bath). In the local case, the weak bath-transmon coupling leads to saturation at 0 dB only for very high temperatures, which are not shown in the inset.

In contrast, their behaviors for intermediate values of temperature are quite different. For a perfectly symmetric global bath, the transmission coefficients would always be equal to 0 dB. However, we know that global bath in the experiment is not perfectly symmetric, due for instance to slightly different anharmonicities. Nonetheless, while the global bath is not perfectly symmetric and the dark subspace is not completely isolated, the fact that the latter is only weakly coupled to the bath is reflected in the structure of the steady state, as the transition coefficients for the $|D\rangle \to |D'\rangle$ transition are closer to 0 dB than in the local case. This can be observed by comparing Fig. 2(b) with Fig. 2(c).

Temperature dependence of the $|D\rangle \to |D'\rangle$ transmission in the global case—There are two reasons for the temperature dependence of the transmission coefficient at the $|D\rangle \to |D'\rangle$ transition frequency for the global bath. First, the spectrum of allowed transitions in the bright subspace is richer than the one shown in Fig. 1(b), and it includes transitions that are close to $f_{DD'}$ in higher excitation manifolds; see SM for more details [45]. Second, no physical system displays perfect symmetry. In our experiment the symmetry is broken by the imprecise location of the transmon pair inside the waveguide and by slightly different anharmonicities of the transmons 2β. In our setup, the transmons have anharmonicities $2\beta_1 \sim -225\ \mathrm{MHz} \cdot 2\pi$ and $2\beta_1 \sim -232\ \mathrm{MHz} \cdot 2\pi$, respectively, for Q_1 and Q_2, i.e., their difference is of the order of $\sim$2.6%. Spectroscopic lines appearing in the system with up to three excitations and the difference in β between the transmons have been taken into account in the model. As one can see from the figure, the observed transmission at $f_{DD'}$ is well described by the curve obtained with the theoretical model.